Open-Circuit Switch Fault Diagnosis of an NPC Converter in a DFIG-Based WECS

S. J. de la Rosa-Mendoza, R. Alvarez-Salas, M. A. Gonzalez-Garcia, G. Espinosa-Perez

***Abstract*—A fault diagnosis method for the power converter of a wind energy conversion system (WECS) is proposed in the present work. The system is composed of a doubly-fed induction generator (DFIG) connected to the grid using a multilevel power electronic converter with a neutral point clamped (NPC) back-to-back (BTB) configuration. Open-circuit faults in the power semiconductor switches are studied in the system under the field-oriented control (FOC) scheme. Only the Rotor Side Converter (RSC) and the Grid Side Converter (GSC) currents, already used in the controller, are considered. The current signals are analyzed using the Discrete Wavelet Transform (DWT) to detect and locate the faults using a digital processing processor (DSP). This algorithm can operate online alongside the control algorithm of the WECS using the same sensors and applies to type III and IV wind turbines.**

***Keywords*—Fault diagnosis, WECS, NPC converter, DFIG, FOC, Discrete Wavelet Transform, DSP.**

I. Introduction

ELECTRIC power generation based on renewable energies is one of the most essential solutions implemented worldwide to reduce greenhouse gases that produce global warming. Exploiting renewable energy has become a fundamental topic of global research and development. In 2023, wind energy reached the historic milestone of 1 TW of installed capacity [1].

In recent years, the doubly-fed induction generator (DFIG) has been one of the most frequently deployed large-scale grid-connected electric machines for modern wind turbines in the high power range (660 kW to 2 MW). They are becoming increasingly acceptable due to their suitability in variable-speed wind power generation systems. DFIGs are more attractive than fixed-speed systems because of their high efficiency, improved power quality, controllability, low operative cost, and maintenance. Another benefit is that the power converter used to operate it manages only a fraction of the total power processed [2].

This work was supported by Programa de becas posdoctorales en la UNAM POSDOC, DGAPA-UNAM, Mexico, and DGAPA-UNAM, grant number [PAPIIT IN109622]. S. J. de la Rosa-Mendoza is with Facultad de Ingeniería, Universidad Nacional Autónoma de México, Ciudad de México, 04510 México (e-mail: sanjouaslp@gmail.com). R. Alvarez-Salas is with Facultad de Ingeniería, Universidad Autónoma de San Luis Potosí, San Luis Potosí, 78290 México (e-mail of corresponding author: ralvarez@uaslp.mx). M. A. Gonzalez-Garcia is with CONAHCYT - Facultad de Ingeniería, Universidad Autónoma de San Luis Potosí, San Luis Potosí, 78290 México (e-mail: mgonzale@uaslp.mx). G. Espinosa-Perez is with Facultad de Ingeniería, Universidad Nacional Autónoma de México, Ciudad de México, 04510 México (e-mail: gerardoe@unam.mx).

Paper submitted to the International Conference on Power Systems Transients (IPST2025) in Guadalajara, Mexico, June 8-12, 2025.

Although wind generation systems based on back-to-back (BTB) converters, using two-level voltage source inverters (VSI), and their control strategies have been extensively studied; there has been growing interest in topologies based on neutral point clamped (NPC) converters for wind turbine systems due to their multilevel topology. The control of NPC converters is already well-developed, with diverse structures and strategies available for their implementation in wind systems [3]. Additionally, multilevel converters, such as NPC, have proven to be effective in renewable energy applications, and their adoption in the wind sector continues to increase due to their advantages over traditional topologies [4].

Failures in wind generation systems have been studied and addressed based on faults occurring in several components like the bearings [5] [6], the generator [7] [8], the sensors [9] and, to a lesser extent, the power converter.

In wind power generation systems, power electronic devices are one of the primary sources of failures, with significant percentages reported in the literature. According to [10], approximately 19% of failures in wind systems are associated with electronic devices. Other studies report similar figures, in [11], it is estimated that this type of failure accounts for 21%. Meanwhile, it is indicated an even higher proportion in [12], reaching 23%. These figures highlight the need to implement effective fault diagnosis techniques and fault-tolerant control, especially in converters used in applications such as wind energy conversion systems (WECS). For instance, in [13], four methods based on machine learning are presented to diagnose open-circuit faults in the BTB converter switches using two-level VSI; the diagnosis time delays obtained range from 1.4 ms to 0.278 s. In [14], a robust fault detection and isolation method for DFIG wind generators based on bond-graph is used with diagnosis time delays ranging from 2 ms to 123 ms in different components.

Simple faults in systems like NPC converters can lead to more complex issues if not properly managed. In [15], it is highlighted that a simple fault, such as an issue with one switch, can trigger a chain of multiple faults if not isolated quickly, compromising the system's stability. Similarly, it is pointed out that a fault in one switch can cause imbalances and overloads, leading to multiple faults [11]. They emphasize the importance of quickly reconfiguring the system to handle such situations. In [16], it is suggested that without adaptive modulation techniques, a simple fault in one switch can escalate to multiple faults, making these strategies crucial.

Fault diagnosis for the NPC BTB converter topology coupled to the DFIG in wind systems is still an open study issue, which has been tried to solve using different approaches.

This paper proposes a fault diagnosis scheme for the NPC BTB converter of a DFIG-based WECS. The scheme is based on the Discrete Wavelet Transform (DWT) applied to the line current signals flowing through the DFIG and implemented on a DSP.

This work is organized as follows: Section II presents the modeling of the WECS and the control scheme used. Section III describes the DWT used as a signal processing basis for the algorithm. Section IV details the proposed algorithm for diagnosing open-circuit switch faults in the NPC converter. The algorithm results and discussion are presented in Section V, and the concluding remarks are stated in Section VI.

II. Modeling and Control of the WECS

This section presents the modeling of the NPC BTB converter and the DFIG. The control scheme is also described.

A. Average model of the NPC BTB converter

First, the model of the NPC BTB converter is presented in the dq reference frame, according to [17] (Fig. 1). The following considerations are assumed: the converter's switching frequency is much greater than the grid frequency, the losses of the switching elements are null, and the three-phase system is balanced. In this way, the model is given by

$$v_{dr} = \frac{u_{dr} v_{DC}}{2} \tag{1}$$

$$v_{qr} = \frac{u_{qr} v_{DC}}{2} \tag{2}$$

$$L\frac{di_{dg}}{dt} = -Ri_{dg} + L\omega i_{qg} + v_{ds} - \frac{u_{dg} v_{DC}}{2} \tag{3}$$

$$L\frac{di_{qg}}{dt} = -Ri_{qg} - L\omega i_{dg} + v_{qs} - \frac{u_{qg} v_{DC}}{2} \tag{4}$$

$$C_1\frac{dv_{c1}}{dt} = \frac{3}{4}(u_{dr}i_{dr} + u_{qr}i_{qr} - u_{dg}i_{dg} - u_{qg}i_{qg}) \tag{5}$$

$$C_2\frac{dv_{c2}}{dt} = -\frac{3}{4}(u_{dr}i_{dr} + u_{qr}i_{qr} - u_{dg}i_{dg} - u_{qg}i_{qg}) \tag{6}$$

where the variables v_{dr}, v_{qr}, v_{ds}, and v_{qs} correspond to the rotor and stator voltages, respectively. Similarly, i_{dr}, i_{qr}, i_{dg}, and i_{qg} represent the currents in the Rotor Side Converter (RSC) and the Grid Side Converter (GSC). Additionally, the elements L and R are link inductance and winding resistance, while u_{dr}, u_{qr}, u_{dg}, and u_{qg} represent the control signals. Furthermore, the DC bus voltage is denoted by v_{DC} and ω is the rotating speed of dq reference frame equal to synchronous speed $\omega_s = 2\pi f_s$ of the DFIG where f_s is the stator frequency.

According to [18], NPC converters represent an efficient and reliable solution for power conversion in high-power WECS. It is highlighted their integration into commercial wind systems such as the FC MV 3000-15000 and INGECON WIND MV100, which operate in the 5 to 15 MW power range, making them among the highest capacity WECS using multilevel converter topologies. NPC converters have become a desirable option in the wind energy sector. They can improve power quality, increase efficiency, and reduce energy losses by lowering switching stress on power devices. As the demand for renewable energy continues to rise, optimizing the design and control of these converters remains critical to ensuring the performance and reliability of modern WECS.

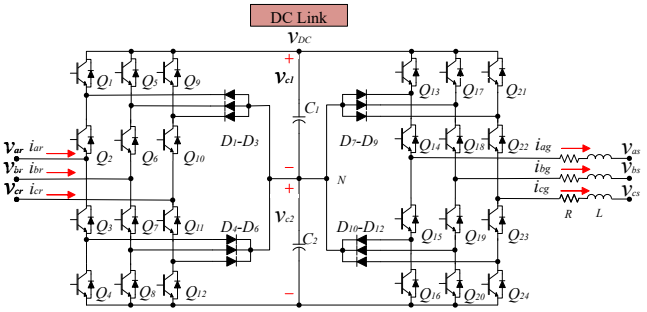

Fig. 1: NPC BTB converter topology.

B. DFIG model

The DFIG model in the dq reference frame, according to [19], is

$$v_{ds} = -r_s i_{sd} - \omega\lambda_{qs} + \frac{d\lambda_{ds}}{dt} \tag{7}$$

$$v_{qs} = -r_s i_{sq} + \omega\lambda_{ds} + \frac{d\lambda_{qs}}{dt} \tag{8}$$

$$v_{dr} = -r_r i_{rd} - s\omega\lambda_{qr} + \frac{d\lambda_{dr}}{dt} \tag{9}$$

$$v_{qr} = -r_r i_{rq} + s\omega\lambda_{dr} + \frac{d\lambda_{qr}}{dt} \tag{10}$$

$$\tau_e = \frac{3p}{4} L_M (i_{qs} i_{dr} - i_{ds} i_{qr}) \tag{11}$$

where the voltages v_{ds}, v_{qs} v_{dr}, v_{qr}, and the currents i_{ds}, i_{qs}, i_{dr} and i_{qr} are electrical variables that are associated with the flow links λ_{ds}, λ_{qs}, λ_{dr} and λ_{qr}, whereas the last expression corresponds to the mechanical variables as a function of the currents, the magnetizing inductance L_M, s is the slip and the number of poles p of the machine.

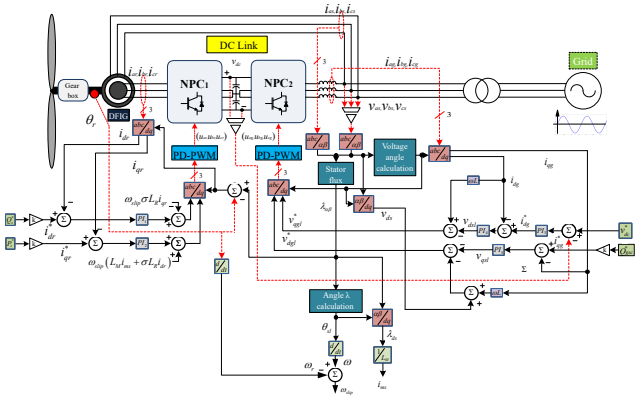

Fig. 2: Wind turbine system based on the DFIG using FOC.

C. Control

According to the diagram of Fig. 2, the NPC converters of the wind generation system have specific control objectives that must be fulfilled in order to operate [20]:

- The converter at the rotor side controls the active and reactive power flowing through the DFIG rotor.
- The converter located at the grid side controls the DC link voltage and the reactive power at the converter's output.

These control objectives are achieved through Field Oriented Control (FOC), which is based on the representation of the generation system using an orthogonal model, in which independent PI controllers can be applied for each control target [19].

Among the pulse width modulation (PWM) techniques that can be used in the NPC converter topology, the phase disposition PWM (PD-PWM) is used in this work [21]. The PD-PWM is commonly used in NPC converters because of its low total harmonic distortion (THD), effective use of the DC-Link, and straightforward implementation. Compared to traditional SPWM techniques, PD-PWM typically achieves THD levels between 3% and 7%, significantly improving output waveform quality. It also enables better DC-Link utilization around 60% to 70%, contributing to more efficient power conversion. One of its main advantages over methods like SVPWM or SHE-PWM is its simplicity; PD-PWM does not require complex mathematical computations, making it well-suited for implementation on mid-range microcontrollers and DSPs. It also provides decent control over the neutral point, helping maintain balance in multilevel systems. These features have led to its widespread adoption in industrial applications, renewable energy systems such as WECS, and electric transportation technologies, where it strikes a practical balance between performance and design complexity [22] [23].

III. Discrete Wavelet Transform

The discrete wavelet transform (DWT) method allows the analysis of non-stationary signals. The DWT with the Haar wavelet is the simplest type and also serves as a point of basic comparison for other existing wavelets [24].

The DWT decomposes the signal into two parts. The first part is the trend signal $\mathbf{a}^1$, and the second one is the fluctuation signal $\mathbf{d}^1$. The first level decomposition of a signal $\mathbf{f} = (f_1, f_2, f_3, ..., f_N)$, where N is a positive even integer number, is represented by

$$\mathbf{f} \overset{H_1}{\longmapsto} (\mathbf{a}^1|\mathbf{d}^1). \tag{12}$$

The trend and fluctuation signals are

$$\mathbf{a}^1 = (a_1, a_2, a_3, ..., a_{N/2}) \qquad \mathbf{d}^1 = (d_1, d_2, d_3, ..., d_{N/2}) \tag{13}$$

The values of $\mathbf{a}^1$ and $\mathbf{d}^1$ are given by

$$a_m = \frac{f_{2m-1} + f_{2m}}{\sqrt{2}} \qquad d_m = \frac{f_{2m-1} - f_{2m}}{\sqrt{2}} \tag{14}$$

where $m = 1, 2, 3, ..., \dfrac{N}{2}$.

The signal $\mathbf{f}$ can be decomposed to multiple levels using the resultant trend signal of each level to perform the subsequent decomposition, for example, the second-level decomposition signals is

$$\mathbf{f} \overset{H_2}{\longmapsto} (\mathbf{a}^2|\mathbf{d}^2|\mathbf{d}^1)$$

Besides the Haar wavelet, many other wavelets exist, like Daubechies 4, which will also be used in this work.

IV. Fault Diagnosis Scheme

The proposed structure of the fault diagnosis method is shown in Fig. 3, where the data is obtained from the DFIG controlled by the FOC, specifically from the RSC and the GSC currents. The data are transferred to a TMS320F28379D digital signal processor (DSP), where the fault diagnosis algorithm based on the DWT is implemented with a sampling frequency of 15.36 kHz, along with the calculations of the mean value of the decomposition signals and thresholds that indicate the existence of a fault. Logic flag signals are activated when a fault diagnosis is performed, depending on the specific fault.

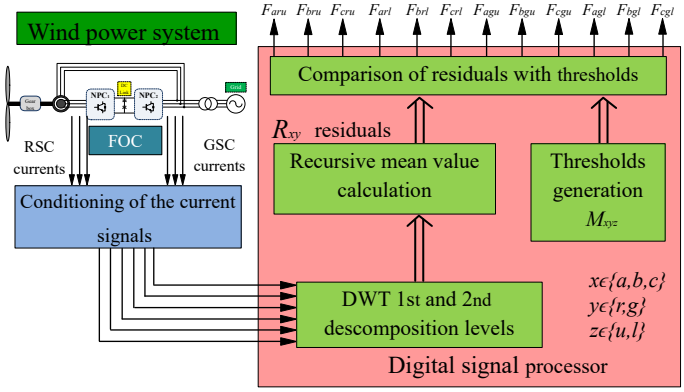

Fig. 3: Fault diagnosis scheme for the DFIG-based wind power system.

Table I shows the parameters of the complete DFIG-based wind generation system under study.

TABLE I: Parameters of the wind generation system.

Parameter	Value
Rated stator voltage (v_a, v_b and v_c)	127 V_{rms}
DC link voltage (V_{DC})	600 V
Link inductance (L)	12.7 mH
Winding resistance (R)	3.2 Ω
Capacitances (C_1 and C_2)	2200 μF
Rated power (P)	1 kW
Switching frequency (f_s)	5 kHz
Mechanical torque (T_m)	0.5 Nm
Moment of inertia (J)	0.089 Kgm^2
Stator inductance (L_S)	27.14 mH
Rotor inductance (L_R)	29.54 mH
Magnetizing inductance (L_M)	150 mH
Stator resistance (r_s)	5.38 Ω
Rotor resistance (r_r)	5.79 Ω
Number of pole pairs (p)	4
Wind speed (V_v)	12 m/s
Pitch angle (θ_p)	15^o

The flowchart of Fig. 4 shows the proposed open-circuit switch fault diagnosis algorithm implemented in the DSP. Only the RSC and GSC currents already used in the controller are considered. The algorithm processes the current signals through the DWT using the Haar and the Daubechies wavelets. The average values are calculated for each current's second-level trend signal. These are compared to the upper and lower thresholds M_{aru}, M_{bru}, M_{cru}, M_{arl}, M_{brl} and M_{crl} for the RSC case, M_{agu}, M_{bgu}, M_{cgu}, M_{agl}, M_{bgl} and M_{cgl} for the GSC case, where the first subscript denotes the phase,

the second one refers to the RSC or GSC, and the third one indicates an upper or lower threshold. The residuals are defined as R_{ar}, R_{br}, R_{cr}, R_{ag}, R_{bg} and R_{cg}, which correspond to the mean value of the second-level trend component of the wavelets in the RSC and GSC line currents.

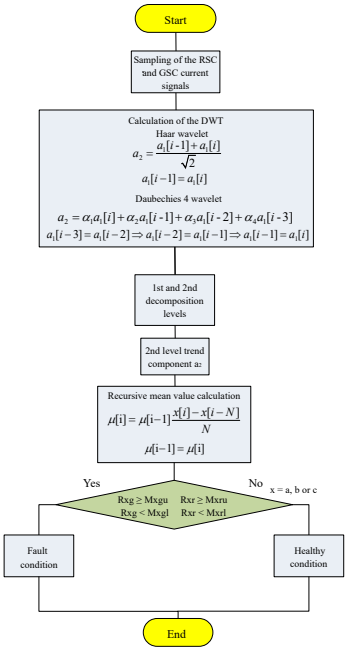

Fig. 4: Flowchart of an open-circuit switch fault diagnosis algorithm in the NPC BTB converter.

To set these thresholds, it is assumed that the operating conditions of the line currents at the RSC, I_{rx}, and GSC, I_{gx}, sides are balanced in regular operation. The nominal current in the rotor can be calculated with the operating conditions of the line voltages V_{rx} in the RSC and the apparent power S_{rx} as

$$I_{rx} = \frac{S_{rx}}{3V_{rx}} \tag{15}$$

and the nominal current in the GSC with the line voltages V_{gx} and the apparent power S_{gx} as

$$I_{gx} = \frac{S_{gx}}{3V_{gx}} \tag{16}$$

with $x \in \{a, b, c\}$.

In this way, the thresholds for the RSC are defined as

$$M_{aru} = M_{bru} = M_{cru} = I_{rn}\Delta_r \tag{17}$$

$$M_{arl} = M_{brl} = M_{crl} = -I_{rn}\Delta_r \tag{18}$$

and in a similar way, but using the nominal operating values on the GSC, the thresholds on the GSC are defined as

$$M_{agu} = M_{bgu} = M_{cgu} = I_{gn}\Delta_g \tag{19}$$

$$M_{agl} = M_{bgl} = M_{cgl} = -I_{gn}\Delta_g \tag{20}$$

where Δ_r and Δ_g are estimated correction factors derived from the observation of the system under faulty and healthy conditions. In each case, if the conditions where the RSC and GSC thresholds are exceeded by the average values of the trend signal, the following binary signals are generated: F_{xru} and F_{xrl} for the RSC case, and F_{xgu} and F_{xgl} for the GSC case, with $x \in \{a, b, c\}$. The following conditions show the activation conditions of each binary signal, which are independent for each phase.

$$\text{Detection in } i_{xr} = \begin{cases} R_{xr} \geq M_{xru} & \rightarrow F_{xru} = 1 \\ R_{xr} < M_{xru} & \rightarrow F_{xru} = 0 \\ R_{xr} \geq M_{xrl} & \rightarrow F_{xrl} = 0 \\ R_{xr} < M_{xrl} & \rightarrow F_{xrl} = 1 \end{cases} \tag{21}$$

$$\text{Detection in } i_{xg} = \begin{cases} R_{xg} \geq M_{xgu} & \rightarrow F_{xgu} = 1 \\ R_{xg} < M_{xgu} & \rightarrow F_{xgu} = 0 \\ R_{xg} \geq M_{xgl} & \rightarrow F_{xgl} = 0 \\ R_{xg} < M_{xgl} & \rightarrow F_{xgl} = 1 \end{cases} \tag{22}$$

If only one indicator is activated, it is classified as a simple fault, corresponding to a single switch fault. On the other hand, if several logic flags are activated simultaneously, they are classified as multiple faults, resulting from faults in more than one switch.

V. Results

Several simple and multiple open-circuit switch fault cases in the NPC converters of the DFIG-based wind power system were tested using the proposed fault diagnosis algorithm. Four cases are presented in detail, and the remaining cases are summarized.

Fig. 5 shows the performance of the fault detection algorithm for an open-circuit fault in the switch Q_1, using the Haar wavelet. As can be observed, this fault affects the line current I_{ar}, and the dark blue line shows the average value of its DWT second-level trend component. Two logic flag signals indicate the instants at which the fault starts (F_0) and when it is detected (F_{aru}). Fault detection is performed in 28 ms, and only the detection signal F_{aru} is activated.

Fig. 6 shows a test in which an open-circuit fault occurs in the switch Q_{13}, but in this case, the algorithm uses the Daubechies 4 wavelet. It can be noted that the fault was detected in 19.5 ms.

Simultaneous multiple open-circuit switch faults were also analyzed using the proposed fault diagnosis algorithm. Fig. 7 presents a test in which an open-circuit fault occurs in both switches Q_1 and Q_6, using, in this case, the Haar wavelet. This multiple fault is correctly detected in 9 ms.

Fig. 8 shows a test involving a multiple fault in two switches (Q_{13} and Q_{18}) of the converter at the stator side. In this case, the flag signals F_{bgu} and F_{agu} determine that multiple faults have occurred on that side of the converter. This multiple fault is detected in 14 ms using the Daubechies 4 wavelet.

Using the proposed fault diagnosis algorithm, several simple and multiple switch fault cases were analyzed. Tables II and III summarize the fault diagnosis delays obtained and the corresponding logic flag signals activated, using the Haar and the Daubechies 4 wavelets. It can be stated that the fault diagnosis delay obtained in each case depends on the exact

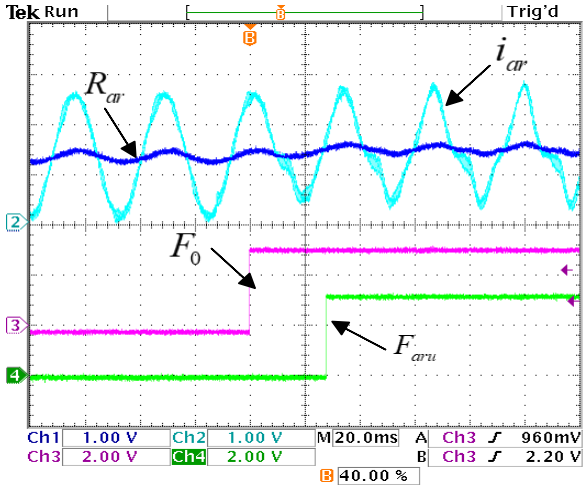

Fig. 5: Fault diagnosis using the second-level Haar DWT applied to the line current under the open-circuit switch fault in Q_1.

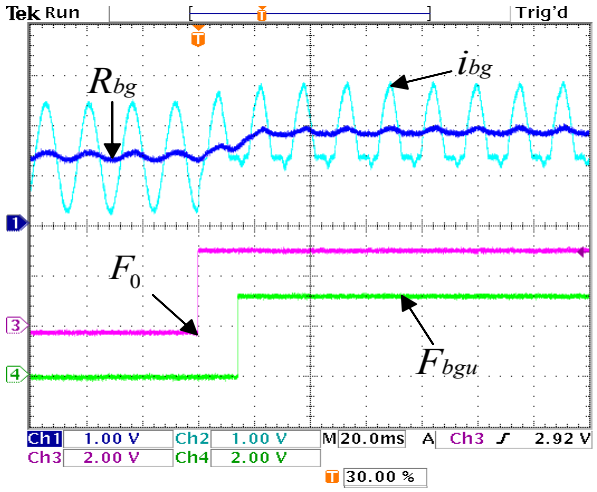

Fig. 6: Fault diagnosis using the second-level Daubechies 4 DWT of the line currents under the open-circuit switch fault in Q_{13}.

moment (electrical angle) at which the fault appears. This is mainly due to the transient response of the mean value calculation and the PD-PWM technique used.

The fault diagnosis delay obtained using the Daubechies 4 wavelet generally shows similar results to those obtained using the Haar wavelet.

Simple faults, such as those occurring in a switch, are more common due to factors like component aging, voltage fluctuations, or extreme operating conditions. These faults are usually easier to detect and handle individually, but they also have the potential to trigger multiple faults if not appropriately managed. The reason for this lies in the interdependence of components in power conversion systems, such as NPC converters, where an initial fault can cause current and voltage

TABLE II: Fault diagnosis delay using the Haar wavelet in ms.

Faults	F_{aru}	F_{bru}	F_{cru}	F_{arl}	F_{brl}	F_{crl}
Q_1	28.0	-	-	-	-	-
Q_3	-	-	-	28.1	-	-
Q_1,Q_6	9.0	-	24.0	-	-	-
Q_3,Q_8	-	-	-	11.0	26.3	-
Faults	F_{agu}	F_{bgu}	F_{cgu}	F_{agl}	F_{bgl}	F_{cgl}
Q_{13}	19.6	-	-	-	-	-
Q_{20}	-	-	-	20.8	-	-
Q_{13},Q_{18}	13.8	17.2	-	-	-	-
Q_{16},Q_{23}	-	-	-	15.0	-	16.0

TABLE III: Fault diagnosis delay using the Daubechies 4 wavelet in ms.

Faults	F_{aru}	F_{bru}	F_{cru}	F_{arl}	F_{brl}	F_{crl}
Q_1	27.9	-	-	-	-	-
Q_3	-	-	-	28.0	-	-
Q_1,Q_6	9.0	-	23.9	-	-	-
Q_3,Q_8	-	-	-	11.0	26.3	-
Faults	F_{agu}	F_{bgu}	F_{cgu}	F_{agl}	F_{bgl}	F_{cgl}
Q_{13}	19.5	-	-	-	-	-
Q_{20}	-	-	-	20.8	-	-
Q_{13},Q_{18}	14.0	17.2	-	-	-	-
Q_{16},Q_{23}	-	-	-	15.2	-	16.0

imbalances, affecting other switches or system components. If the fault is not isolated or corrected in time, these imbalances can lead to a chain failure, compromising the system's overall stability.

Finally, the subsequent actions for handling faults in NPC converters after the fault occurrence are described in the following: 1) Fault identification and isolation, which focuses on detecting and locating faults in components like power switches, isolating them to prevent further damage [25], [26]. 2) Control reconfiguration is all about adapting the system's control after a fault, adjusting settings, or changing operation modes to keep the converter stable [27], [28]. 3) Fault-tolerant control ensures the converter keeps running even after a fault, using techniques like adaptive modulation or reconfiguring the control [26], [28]. 4) Recovery strategies outline actions that bring the system back to operational status, such as reducing load or reconfiguring resources to maintain functionality [25], [29]. Table IV highlights key strategies for handling faults in NPC converters.

Generally, the response times after fault detection in an NPC converter vary depending on the action taken, but in most cases, these actions must be executed exceptionally quickly to avoid damage and ensure system stability. The fault identification and isolation should be nearly instantaneous, occurring in less than one second in most cases. Control reconfiguration and fault-tolerant control can take from a few seconds to tens of milliseconds, while recovery strategies also require very short times, mostly less than one second. These times are critical to maintaining continuous and efficient operation of power systems, especially in renewable energy applications and industrial sectors where reliability is crucial.

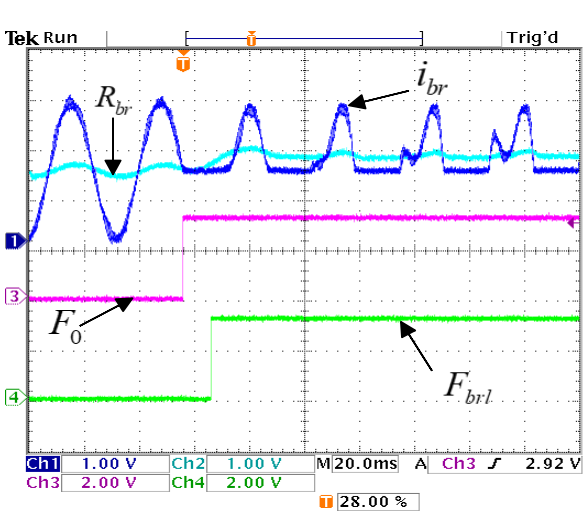

(a) Fault detection.

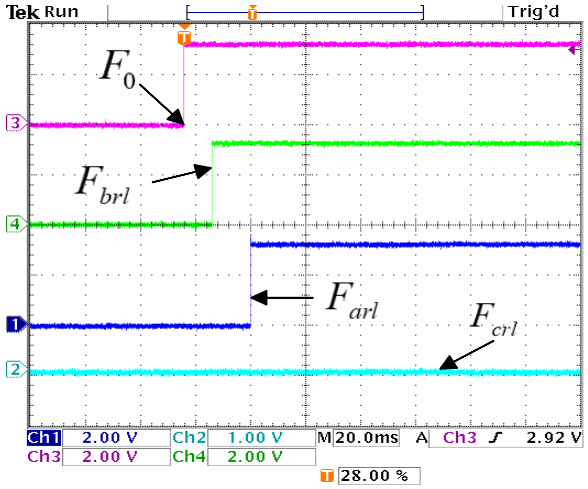

(b) Fault flag signals.

Fig. 7: Fault diagnosis using the second-level Haar DWT of the line currents under open-circuit switch faults in Q_1 and Q_6.

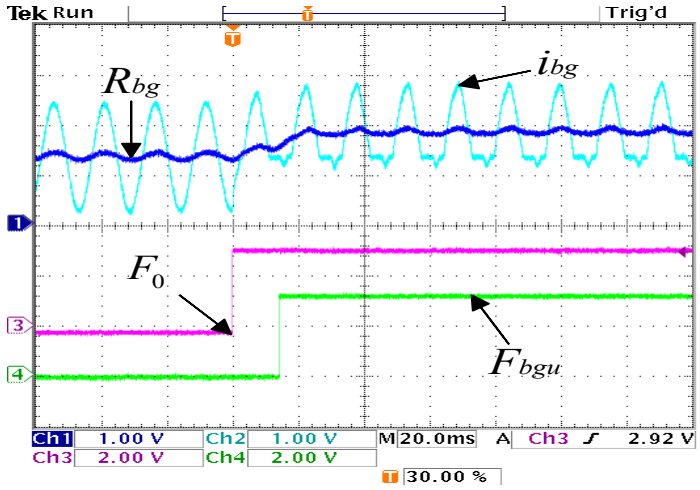

(a) Fault detection.

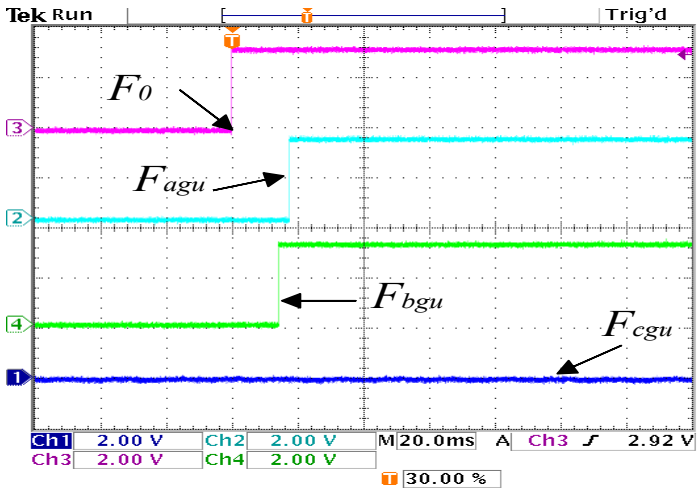

(b) Fault flag signals.

Fig. 8: Fault diagnosis using the second-level Daubechies 4 DWT of the line currents under open-circuit switch faults in Q_{13} and Q_{18}.

VI. Conclusions

This work presents the development of a fault diagnosis algorithm based on the DWT with the Haar and Daubechies 4 wavelets for a DFIG-based wind turbine generation system operating with a multilevel NPC BTB converter and field-oriented control.

The fault diagnosis was done in a DSP device, and the algorithm can operate online with the control system. The faults studied consider open-circuit faults in the converter's power switches. Four relevant cases are presented in detail, and a complete study of several cases is summarized. The analysis was carried out using the RSC and GSC current signals, obtaining reasonably short fault diagnosis delays ranging from 9 ms to 28.1 ms.

Identifying faults in all the converter switches as single faults was feasible. However, in some multiple fault cases, detection is possible but not location with this method. For instance, faults involving the switches of a particular branch show the same behavior as simple faults.

It is highlighted that since the fault diagnosis scheme depends only on current signals, it can also be applied to type IV wind turbines.

References

[1] GWEC, Global Wind Report 2023, [Online]. Available: https://gwec.net/globalwindreport2023/.

TABLE IV: Actions to be taken after a fault occurrence in an NPC converter.

Action	Description	Reference	Response Time
Fault identification and isolation	- Activation of overcurrent and overvoltage protection. - Isolation of the faulty switch. - Analysis of current and voltage signals for fault diagnosis.	[25], [26]	< 1 s
Control reconfiguration	- Adjustment of PWM modulation. - Operation in degraded mode (switching from three-level to two-level operation). - Modification of voltage and current references.	[27], [28]	2 s - 5 s
Fault-tolerant control	- Neutral-point balancing to minimize distortion. - Current redirection to other devices. - Control algorithms compensating for faults without additional hardware.	[26], [28]	1 ms - 1 s
Recovery strategies	- Decision to operate in reduced power mode or shut down the converter. - Activation of redundant systems if available. - Sending alerts for preventive maintenance.	[25], [29]	< 1 s

[2] T. Burton, N. Jenkins E. Bossanyi, D. Sharp, and M. Graham, Wind energy handbook, 3rd ed., John Wiley & Sons, 2021.

[3] H. A. Hussain, "Enhanced control of back-to-back converters in wind energy conversion systems using two-degree-of-freedom (2DOF) PI controllers," *Electronics*, vol. 12, no. 20, p. 4221, 2023.

[4] A. Mansouri, A. El Magri, R. Lajouad, I. El Myasse, F. Giri, *et al.*, "Wind energy based conversion topologies and maximum power point tracking: A comprehensive review and analysis," *e-Prime - Advances in Electrical Engineering, Electronics and Energy*, vol. 6, p. 100351, 2023.

[5] Xi Chen, Wei Xu, Yi Liu, and Md. Rabiul Islam, "Bearing Corrosion Failure Diagnosis of Doubly Fed Induction Generator in Wind Turbines Based on Stator Current Analysis," *IEEE Transactions on Industrial Electronics*, vol. 67, no. 5, pp. 3419-3430, May 2020.

[6] Hong Tang, Hong-Liang Dai and Yi Du, "Bearing Fault Detection for Doubly fed Induction Generator Based on Stator Current," *IEEE Transactions on Industrial Electronics*, vol. 69, no. 5, pp. 5267-5276, May 2022.

[7] Estefania Artigao, Andrés Honrubia-Escribano and Emilio Gómez-Lázaro, "In-Service Wind Turbine DFIG Diagnosis Using Current Signature Analysis," *IEEE Transactions on Industrial Electronics*, vol. 67, no. 3, pp. 2262-2271, March 2020.

[8] Ester Hamatwi, Paul Barendse and Azeem Khan, "A Case for Micromachines in Laboratory-Based DFIG Wind Turbine Systems for Fault Studies," *IEEE Transactions on Industry Applications*, vol. 59, no. 2, pp. 1754-1764, March-April 2023.

[9] Mohamed-Amine Yahiaoui, Michel Kinnaert and Johan Gyselinck, "Augmented-State-Observer-Based Diagnostics of Open-Circuit and Sensor Faults in DFIG Wind Turbines," *IEEE Transactions on Power Electronics*, vol. 38, no. 12, pp. 16085-16099, Dec. 2023.

[10] J. Liang, K. Zhang, A. Al-Durra, S. Muyeen, and D. Zhou, "A state-of-the-art review on wind power converter fault diagnosis," *Energy Reports*, vol. 8, pp. 5341–5369, 2022.

[11] K. Nallathambi *et al.*, "An extensive review on fault detection and fault-tolerant control of multilevel inverter with applications," *International Journal of Renewable Energy Research (IJRER)*, vol. 12, no. 2, pp. 768–798, 2022.

[12] Z. Gao and X. Liu, "An overview on fault diagnosis, prognosis and resilient control for wind turbine systems," *Processes*, vol. 9, no. 2, p. 300, 2021.

[13] Z. Y. Xue, K. S. Xiahou, M. S. Li, T. Y. Ji, and Q. H. Wu, "Diagnosis of Multiple Open-Circuit Switch Faults Based on Long Short-Term Memory Network for DFIG-Based Wind Turbine Systems," *IEEE Journal of Emerging and Selected Topics in Power Electronics*, vol. 8, no. 3, pp. 2600-2610, Sept. 2020.

[14] Aslan Mojallal and Saeed Lotfifard, "DFIG wind generators fault diagnosis considering parameter and measurement uncertainties," *IEEE Transactions on Sustainable Energy*, vol. 9, no. 2, pp. 792-804, April 2018.

[15] J. A. Pecina Sánchez, D. U. Campos-Delgado, D. R. Espinoza-Trejo, A. A. Valdez-Fernández, and C. H. De Angelo, "Fault diagnosis in grid-connected PV NPC inverters by a model-based and data processing combined approach," *IET Power Electronics*, vol. 12, no. 12, pp. 3254–3264, 2019.

[16] M. Farhadi, M. Abapour, and M. Sabahi, "Failure analysis and reliability evaluation of modulation techniques for neutral point clamped inverters - a usage model approach," *Engineering Failure Analysis*, vol. 71, pp. 90–104, 2017.

[17] Ned Mohan and Tore M. Undeland, Power electronics: converters, applications, and design, John Wiley & Sons, 2007.

[18] S. Rajendran, M. Diaz, R. Cárdenas, E. Espina, E. Contreras, and J. Rodriguez, "A review of generators and power converters for multi-MW wind energy conversion systems," *Processes*, vol. 10, no. 11, p. 2302, 2022.

[19] Bin Wu, Yongqiang Lang, Navid Zargario, and Samir Kouro, Power conversion and control of wind energy systems, John Wiley & Sons, 2011.

[20] Olimpo Anaya-Lara, Nick Jenkins, Janaka Ekanayake, Phill Cartwright, and Michael Hughes, Wind energy generation: modelling and control, John Wiley & Sons, 2011.

[21] D. Grahame Holmes and Thomas A. Lipo, Pulse width modulation for power converters: principles and practice, John Wiley & Sons, 2003.

[22] J. Rodriguez, S. Bernet, P. K. Steimer, and I. E. Lizama, "A survey on neutral-point-clamped inverters," *IEEE transactions on Industrial Electronics*, vol. 57, no. 7, pp. 2219–2230, 2009.

[23] R. Sarker, "Phase disposition PWM (PD-PWM) technique to minimize WTHD from a three-phase NPC multilevel voltage source inverter," in *2020 IEEE 1st International Conference for Convergence in Engineering (ICCE)*, pp. 220–224, IEEE, 2020.

[24] James S. Walker, A primer on wavelets and their scientific applications, CRC Press, 2008.

[25] F. Wang, R. Lai, X. Yuan, F. Luo, R. Burgos, and D. Boroyevich, "Failure-mode analysis and protection of three-level neutral-point-clamped PWM voltage source converters," *IEEE Transactions on industry applications*, vol. 46, no. 2, pp. 866–874, 2010.

[26] K.-H. Chao and C.-H. Ke, "Fault diagnosis and tolerant control of three-level neutral-point clamped inverters in motor drives," *Energies*, vol. 13, no. 23, p. 6302, 2020.

[27] U.-M. Choi, J.-S. Lee, F. Blaabjerg, and K.-B. Lee, "Open-circuit fault diagnosis and fault-tolerant control for a grid-connected NPC inverter," *IEEE Transactions on Power Electronics*, vol. 31, no. 10, pp. 7234–7247, 2015.

[28] A. Ventosa-Cutillas, P. Montero-Robina, F. Umbría, F. Cuesta, and F. Gordillo, "Integrated control and modulation for three-level NPC rectifiers," *Energies*, vol. 12, no. 9, p. 1641, 2019.

[29] J. Huang, F. Bai, Q. Yang, and S. Ren, "A fault-tolerant control strategy for three-level grid-connected NPC inverters after single-arm failure with optimized SVPWM," *Energies*, vol. 16, no. 23, p. 7863, 2023.